



Optics Letters

1.53 W all-solid-state nanosecond pulsed mid-infrared laser at 6.45 μm

ZE LV,^{1,2} YU SHEN,^{1,3,*} NAN ZONG,^{1,3,5} QI BIAN,^{1,3} ER-PENG WANG,⁴ JIN-QUAN CHANG,^{1,2} YONG BO,^{1,3} DA-FU CUI,^{1,3} AND QIN-JUN PENG^{1,3}

¹Key Lab of Solid State Laser, Technical Institute of Physics and Chemistry, Chinese Academy of Sciences, Beijing 100190, China

²University of Chinese Academy of Sciences, Beijing 100190, China

³Key Lab of Functional Crystal and Laser Technology, Technical Institute of Physics and Chemistry, Chinese Academy of Sciences, Beijing 100190, China

⁴Institute of Optical Physics and Engineering Technology, Qilu Zhongke, Jinan 250000, China

⁵e-mail: zongnan@mail.ipc.ac.cn

*Corresponding author: shenyu@mail.ipc.ac.cn

Received 20 October 2021; revised 12 January 2022; accepted 14 January 2022; posted 14 January 2022; published 4 March 2022

A compact and robust all-solid-state mid-infrared (MIR) laser at 6.45 μm with high average output power and near-Gaussian beam quality is demonstrated. A maximum output power of 1.53 W with a pulse width of approximately 42 ns at 10 kHz is achieved using a ZnGeP₂ (ZGP) optical parametric oscillator (OPO). This is the highest average power at 6.45 μm of any all-solid-state laser to the best of our knowledge. The average beam quality factor is measured to be $M^2 = 1.19$. Moreover, high output power stability is confirmed, with a power fluctuation of less than 1.35% rms over 2 h, and the laser can run efficiently for more than 500 h in total. Using this 6.45 μm pulse as a radiation source, ablation of animal brain tissue is tested. Furthermore, the collateral damage effect is theoretically analyzed for the first time, to the best of our knowledge, and the results indicate that this MIR laser has excellent ablation ability, making it a potential replacement for free electron lasers. © 2022 Optica Publishing Group

<https://doi.org/10.1364/OL.446336>

Mid-infrared (MIR) 6.45 μm laser radiation has potential applications in high-precision medicine fields due to its advantages of a substantial ablation rate and minimal collateral damage [1]. Free electron lasers (FELs), strontium vapor lasers, gas Raman lasers, and solid-state lasers based on an optical parametric oscillator (OPO) or difference frequency generation (DFG) are commonly used 6.45 μm laser sources. However, the high cost, large size, and complex structure of FELs restrict their application. Strontium vapor lasers and gas Raman lasers can obtain the target bands, but both have poor stability, short service lives, and require complex maintenance. Studies showed that 6.45 μm solid-state lasers produce a smaller thermal damage range in biological tissues and that their ablation depth is deeper than those of a FEL under the same conditions, which verified that they can be used as an effective alternative to FELs for biological tissue ablation [2]. In addition, solid-state lasers have the advantages of a compact structure, good stability, and

tabletop operation, making them promising tools for obtaining a 6.45 μm light source.

As is well known, nonlinear infrared crystals play an important role in the frequency conversion process used to achieve high-performance MIR lasers. Compared to oxide infrared crystals with a 4 μm cut-off edge, non-oxide crystals are well suited to generating MIR lasers. These crystals include most of the chalcogenides, such as AgGaS₂ (AGS) [3,4], LiInS₂ (LIS) [5,6], LiInSe₂ (LISE) [7], BaGa₄S₇ (BGS) [8,9], and BaGa₄Se₇ (BGSe) [10–12], as well as the phosphorus compounds CdSiP₂ (CSP) [13–16] and ZnGeP₂ (ZGP) [17]; the latter two both have relatively large nonlinear coefficients. For instance, MIR radiation can be obtained using CSP-OPOs. However, most CSP-OPOs operate on an ultrashort (pico- and femtosecond) time scale and are synchronously pumped by approximately 1 μm mode-locked lasers. Unfortunately, these synchronously pumped OPO (SPOPO) systems have a complex setup and are costly. Their average powers are also lower than 100 mW at around 6.45 μm [13–16]. Compared with CSP crystal, ZGP has a higher laser damage threshold (60 MW/cm²), a higher thermal conductivity (0.36 W/cm K), and a comparable nonlinear coefficient (75 pm/V). Therefore, ZGP is an excellent MIR nonlinear optical crystal for high-power or high-energy applications [18–22]. For example, a flat-flat cavity ZGP-OPO with a tuning range of 3.8–12.4 μm pumped by a 2.93 μm laser was demonstrated. The maximum single-pulse energy of the idler light at 6.6 μm was 1.2 mJ [20]. For the specific wavelength of 6.45 μm , a maximum single-pulse energy of 5.67 mJ at a repetition frequency of 100 Hz was achieved using a non-planar ring OPO cavity based on a ZGP crystal. With a repetition frequency of 200 Hz, an average output power of 0.95 W was reached [22]. As far as we are aware, this is the highest output power achieved at 6.45 μm . Existing studies suggest that a higher average power is necessary for effective tissue ablation [23]. Therefore, the development of a practical high-power 6.45 μm laser source would be of great significance in the promotion of biological medicine.

In this Letter, we report a simple, compact all-solid-state MIR 6.45 μm laser that has a high average output power and is based on a ZGP-OPO pumped by a nanosecond (ns)-pulse 2.09 μm

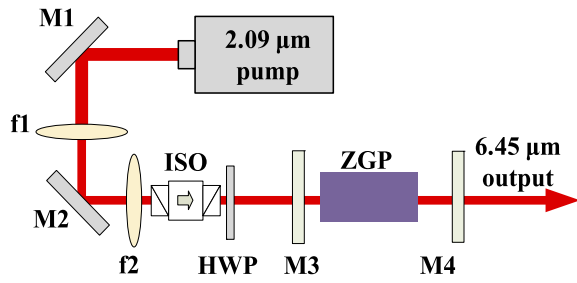


Fig. 1. Experimental arrangement of the 6.45 μm ZGP-OPO system.

laser. The maximum average output power of the 6.45 μm laser is up to 1.53 W with a pulse width of approximately 42 ns at a repetition frequency of 10 kHz, and it has excellent beam quality. The ablating effect of the 6.45 μm laser on animal tissue is investigated. This work shows that the laser is an effective approach for actual tissue ablation, as it acts as a laser scalpel.

The experimental setup is sketched in Fig. 1. The ZGP-OPO is pumped by a home-made LD-pumped 2.09 μm Ho:YAG laser that delivers 28 W of average power at 10 kHz with a pulse duration of approximately 102 ns (FWHM) and an average beam quality factor M^2 of approximately 1.7. M1 and M2 are two 45° mirrors with a coating that is highly reflective at 2.09 μm . These mirrors enable direction control of the pump beam. Two focusing lenses ($f_1 = 100$ mm, $f_2 = 100$ mm) are applied for beam collimation with a beam diameter of about 3.5 mm in the ZGP crystal. An optical isolator (ISO) is used to prevent the pump beam returning to the 2.09 μm pump source. A half-wave plate (HWP) at 2.09 μm is used to control the polarization of the pump light. M3 and M4 are OPO cavity mirrors, with flat CaF₂ used as the substrate material. The front mirror M3 is anti-reflection coated (98%) for the pump beam and high-reflection coated (98%) for the 6.45 μm idler and 3.09 μm signal waves. The output mirror M4 is highly reflective (98%) at 2.09 μm and 3.09 μm and allows partial transmission of the 6.45 μm idler.

The ZGP crystal is cut at $\theta = 77.6^\circ$ and $\varphi = 45^\circ$ for type-II phase matching [2090.0 (o) \rightarrow 6450.0 (o) + 3091.9 (e)], which is more suitable for a specific wavelength and yields parametric light with a narrower linewidth compared with type-I phase matching. The dimensions of the ZGP crystal are 5 mm \times 6 mm \times 25 mm, and it is polished and anti-reflection coated on both end facets for the above three waves. It is wrapped in indium foil and fixed in a copper heat sink with water cooling ($T = 16^\circ$). The cavity length is 27 mm. The round-trip time of the OPO is 0.537 ns for the pump laser. We tested the damage threshold of the ZGP crystal by the R-on-1 method [17]. The damage threshold of the ZGP crystal was measured to be 0.11 J/cm² at 10 kHz in the experiment, corresponding to a peak power density of 1.4 MW/cm², which is low due to the relatively poor coating quality. The output power of the generated idler light is measured by an energy meter (D, OPHIR, 1 μW to 3 W), and the wavelength of the signal light is monitored by a spectrometer (APE, 1.5–6.3 μm).

In order to obtain a high output power of 6.45 μm , we optimize the design of the parameters of the OPO. A numerical simulation is carried out based on three-wave mixing theory and paraxial propagation equations [24,25]; in the simulation, we employ the parameters corresponding to the experimental conditions and assume an input pulse with a Gaussian profile in space and time. The relationship between OPO output mirror

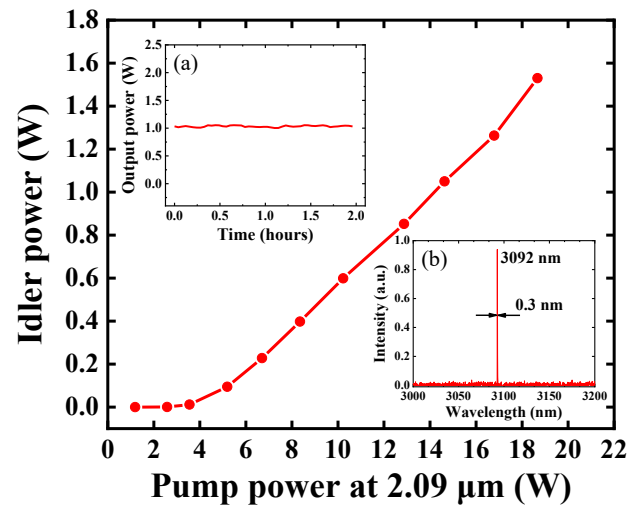


Fig. 2. Output power at 6.45 μm versus pump power at 2.09 μm . Insets: (a) signal spectrum of the ZGP-OPO; (b) measured power stability of the idler at 6.45 μm over 2 h.

transmittance, pump power intensity, and output efficiency is optimized by manipulating the pump beam density in the cavity to achieve higher output power while simultaneously avoiding damage to the ZGP crystal and the optical elements. Thus, the highest pump power is limited to be about 20 W for ZGP-OPO operation. Simulated results show that while an optimal output coupler with a transmittance of 50% is utilized, the maximum peak power density is only 2.6×10^5 W/cm² in the ZGP crystal, and an average output power of more than 1.5 W can be obtained.

Figure 2 shows the relationship between the measured output power of the idler at 6.45 μm and the incident pump power. It can be seen from Fig. 2 that the output power of the idler increases monotonously with the incident pump power. The pump threshold corresponds to an average pump power of 3.55 W. A maximum idler output power of 1.53 W is achieved at a pump power of approximately 18.7 W, which corresponds to an optical-to-optical conversion efficiency of approximately 8.20% and a quantum conversion efficiency of 25.31%. For long-term safety, the laser is operated at near to 70% of its maximum output power. The power stability is measured at an output power of 1 W, as shown in inset (a) in Fig. 2. It is found that the measured power fluctuation is less than 1.35% rms in 2 h, and that the laser can operated efficiently for more than 500 h in total.

The wavelength of the signal wave is measured instead of that of the idler due to the limited wavelength range of the spectrometer (APE, 1.5–6.3 μm) used in our experiment. The measured signal wavelength is centered at 3.09 μm and the line width is approximately 0.3 nm, as shown in inset (b) of Fig. 2. The central wavelength of the idler is then deduced to be 6.45 μm . The pulse width of the idler is detected by a photodetector (Thorlabs, PDAVJ10) and recorded by a digital oscilloscope (Tektronix, 2 GHz). A typical oscilloscope waveform is shown in Fig. 3 and displays a pulse width of approximately 42 ns. The pulse width is 41.18% narrower for the 6.45 μm idler compared to the 2.09 μm pump pulse due to the temporal gain narrowing effect of the nonlinear frequency conversion process. As a result, the corresponding idler pulse peak power is 3.56 kW. The beam quality factor of the 6.45 μm idler is measured with a laser beam

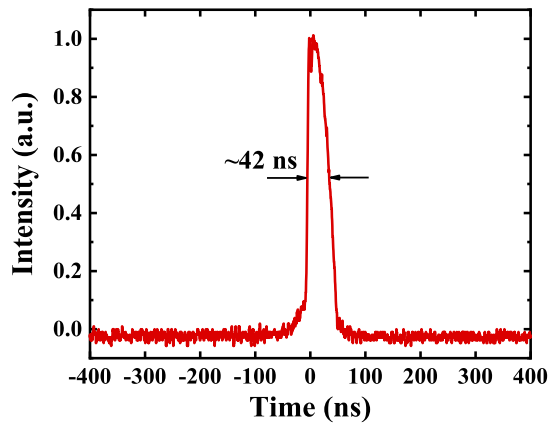


Fig. 3. Pulse width measurement of the idler light at 6.45 μm .

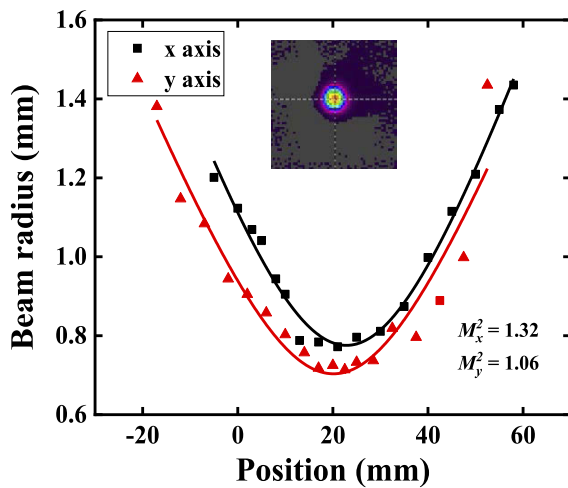


Fig. 4. Beam quality factor measurement of the 6.45 μm idler. Inset: 2D beam intensity profile.

analyzer (Spiricon, M2-200-PIII) at 1 W of output power, as shown in Fig. 4. The measured values of M_x^2 and M_y^2 are 1.32 and 1.06 along the x axis and the y axis, respectively, corresponding to an average beam quality factor of $M^2 = 1.19$. The inset of Fig. 4 shows the two-dimensional (2D) beam intensity profile, which has a near-Gaussian spatial mode.

To verify that the 6.45 μm pulse provides effective ablation, a proof-of-principle experiment involving laser ablation of porcine brain is carried out. An $f = 50$ lens is employed to focus the 6.45 μm pulse beam to a waist radius of about 0.75 mm. The position to be ablated on the porcine brain tissue is placed at the focus of the laser beam. The surface temperature (T) of the biological tissue as a function of the radial location r is measured by a thermocamera (FLIR A615) synchronously during the ablation process. The irradiation durations are 1, 2, 4, 6, 10, and 20 s at a laser power of 1 W. For each irradiation duration, six sample positions are ablated: $r = 0, 0.62, 0.703, 1.91, 3.05,$ and 4.14 mm along the radial direction with respect to the center point of the irradiation position, as shown in Fig. 5. The squares are the measured temperature data. It is found in Fig. 5 that the surface temperature at the ablation position on the tissue increases with increasing irradiation duration. The highest temperatures T at the center point $r = 0$ are 132.39, 160.32, 196.34,

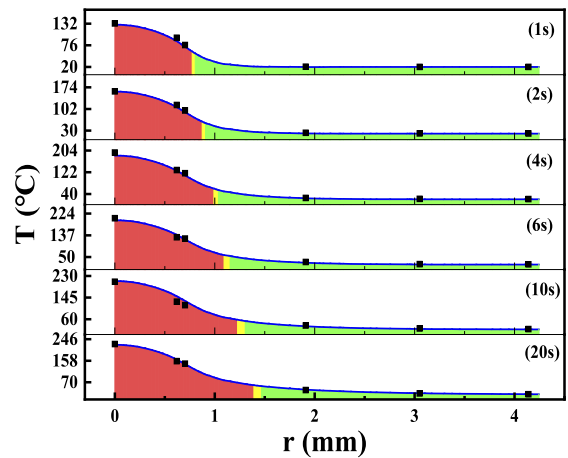


Fig. 5. Temperature distribution on the ablated tissue surface with respect to the center point of the irradiation position for different irradiation durations. The black squares are the measured data. The solid curves are the simulated results. The left shaded zone is where the temperature T exceeds 60°C. The middle shaded zone is where $55^\circ\text{C} \leq T < 60^\circ\text{C}$, and the right shaded zone is where $T < 55^\circ\text{C}$.

Table 1. Parameters of Porcine Brain Tissue Used in the Simulation of the Temperature Distribution

Parameter	Value
Density	1050 kg/m ³
Heat capacity	3700 J/(kg K)
Heat conductivity coefficient	0.5 W/(m K)
Reflection coefficient	0.3
Absorption coefficient	23 cm ⁻¹
Scattering coefficient	72 cm ⁻¹
Heat transfer coefficient	10 W/(m ² K)

205.57, 206.95, and 226.05°C for irradiation durations of 1, 2, 4, 6, 10, and 20 s, respectively.

To analyze the collateral damage, the temperature distribution on the ablated tissue surface is simulated. This is carried out according to the thermal conduction theory for biological tissue [26] and the theory of laser propagation in biological tissue [27] combined with the optical parameters of porcine brain [28]. The simulation is performed with the assumption of an input Gaussian beam. Since the biological tissue used in the experiment is isolated porcine brain tissue, the influence of blood and metabolism on the temperature is ignored, and the porcine brain tissue is simplified into the shape of a cylinder for simulation. The parameters used in the simulation are summarized in Table 1.

The solid curves shown in Fig. 5 are the simulated radial temperature distributions with respect to the ablation center on the tissue surface for the six different irradiation durations. They exhibit a Gaussian temperature profile from the center to the periphery. It is evident from Fig. 5 that the experimental data agree well with the simulated results.

It is also apparent from Fig. 5 that the simulated temperature at the center of the ablation position increases as the irradiation duration increases for each irradiation. Previous research has shown that the cells in the tissue are perfectly safe at temperatures below 55°C, which means that cells remain active in the green zones ($T < 55^\circ\text{C}$) of the curves in Fig. 5. The yellow

zone of each curve ($55^{\circ}\text{C} \leq T < 60^{\circ}\text{C}$) is defined as the collateral damage zone in our paper, as the activity of the cells cannot be identified. When the temperature exceeds 60°C , the protein and collagen in biological tissues is denatured, leading to tissue coagulation and cell necrosis [29]. As a result, the cells die in the red zone ($T \geq 60^{\circ}\text{C}$). It can be observed in Fig. 5 that the simulated ablation radii at $T = 60^{\circ}\text{C}$ are 0.774, 0.873, 0.993, 1.071, 1.198, and 1.364 mm, respectively, for irradiation durations of 1, 2, 4, 6, 10, and 20 s, while the simulated ablation radii at $T = 55^{\circ}\text{C}$ are 0.805, 0.908, 1.037, 1.134, 1.271, and 1.456 mm, respectively.

Upon quantitatively analyzing the ablation effect, the area with dead cells is found to be 1.882, 2.394, 3.098, 3.604, 4.509, and 5.845 mm^2 for 1, 2, 4, 6, 10, and 20 s of irradiation, respectively. The area with collateral damage area is found to be 0.003, 0.004, 0.006, 0.013, 0.017, and 0.027 mm^2 . It can be seen that the laser ablation zones and the collateral damage zones increase with the irradiation duration. We define the collateral damage ratio to be the ratio of the collateral damage area at $55^{\circ}\text{C} \leq T < 60^{\circ}\text{C}$ to the laser ablation area at $T \geq 60^{\circ}\text{C}$. The collateral damage ratio is found to be 8.17%, 8.18%, 9.06%, 12.11%, 12.56%, and 13.94% for different irradiation times, which means that the collateral damage of the ablated tissues is small. Therefore, comprehensive experimental data and simulation results show that this compact, high-power, all-solid-state $6.45 \text{ }\mu\text{m}$ ZGP-OPO laser provides effective ablation of biological tissues.

In conclusion, we have demonstrated a compact, high-power, all-solid-state MIR pulsed $6.45 \text{ }\mu\text{m}$ laser source based on a ns ZGP-OPO approach. A maximum average power of 1.53 W was obtained with a peak power of 3.65 kW and an average beam quality factor of $M^2 = 1.19$. Using this $6.45 \text{ }\mu\text{m}$ MIR radiation, a proof-of-principle experiment on the laser ablation of tissue was performed. The temperature distribution on the ablated tissue surface was experimentally measured and theoretically simulated. The measured data agreed well with the simulated results. Moreover, the collateral damage was theoretically analyzed for the first time. These results verify that our tabletop MIR pulse laser at $6.45 \text{ }\mu\text{m}$ offers effective ablation of biological tissues and has great potential to be a practical tool in medical and biological science, as it could replace a bulky FEL as a laser scalpel.

Funding. National Natural Science Foundation Programs of China (11504389, 51890864); Technical Institute of Physics and Chemistry of the Chinese Academy of Sciences.

Acknowledgment. The authors would like to acknowledge Prof. Glenn Edwards at the Physics Department in Duke University for productive discussions and assistance with the details in Mid-IR laser ablation during the course of this work. The authors also thank the support of ZGP crystal from Chengdu Dien Photoelectric Technology Co., Ltd. (DIEN TECH).

Disclosures. The authors declare no conflicts of interest.

Data availability. Data underlying the results presented in this paper are not publicly available at this time but may be obtained from the authors upon reasonable request.

REFERENCES

- G. Edwards, R. Logan, M. Copeland, L. Reinisch, J. Davidson, B. Johnson, R. Maciunas, M. Mendenhall, R. Ossoff, J. Tribble, J. Werkhaven, and D. Oday, *Nature* **371**, 416 (1994).
- M. A. Mackanos, D. Simanovskii, K. M. Joos, H. A. Schwettman, and E. D. Jansen, *Lasers Surg. Med.* **39**, 230 (2007).
- K. L. Vodopyanov, J. P. Maffetone, I. Zwieback, and W. Ruderman, *Appl. Phys. Lett.* **75**, 1204 (1999).
- K. Kato, *IEEE J. Quantum Electron.* **20**, 698 (1984).
- F. Rotermund, V. Petrov, F. Noack, L. Isaenko, A. Yelisseyev, and S. Lobanov, *Appl. Phys. Lett.* **78**, 2623 (2001).
- W. D. Chen, E. Pouillet, J. Burie, D. Boucher, M. W. Sigrist, J. J. Zondy, L. Isaenko, A. Yelisseyev, and S. Lobanov, *Appl. Opt.* **44**, 4123 (2005).
- A. Tyazhev, G. Marchev, V. Vedenyapin, D. Kolker, A. Yelisseyev, S. Lobanov, L. Isaenko, J.-J. Zondy, and V. Petrov, *Proc. SPIE* **7582**, 75820E (2010).
- A. Tyazhev, D. Kolker, G. Marchev, V. Badikov, D. Badikov, G. Shevyrdyaeva, V. Panyutin, and V. Petrov, in *2012 Conference on Lasers and Electro-Optics*, OSA Technical Digest (2012), paper CTh1B.4.
- J.-J. Zhang, F. Yang, S.-D. Yang, S.-H. Fang, X.-J. Wang, Q.-J. Peng, N. Ye, and Z.-Y. Xu, *Infrared Phys. Technol.* **111**, 103571 (2020).
- J. Zhang, Q. Wang, J. Hao, H. Liu, J. Yao, Z. Li, J. Liu, and K. F. Mak, *Opt. Express* **28**, 37903 (2020).
- F. Yang, J.-Y. Yao, H.-Y. Xu, F.-F. Zhang, N.-X. Zhai, Z.-H. Lin, N. Zong, Q.-J. Peng, J.-Y. Zhang, D.-F. Cui, Y.-C. Wu, C.-T. Chen, and Z.-Y. Xu, *IEEE Photonics Technol. Lett.* **27**, 1100 (2015).
- N. Y. Kostyukova, A. A. Boyko, V. Badikov, D. Badikov, G. Shevyrdyaeva, V. Panyutin, G. M. Marchev, D. B. Kolker, and V. Petrov, *Opt. Lett.* **41**, 3667 (2016).
- S. Chaitanya Kumar, K. T. Zawilski, P. G. Schunemann, and M. Ebrahim-Zadeh, *Opt. Lett.* **42**, 3606 (2017).
- A. Peremans, D. Lis, F. Cecchet, P. G. Schunemann, K. T. Zawilski, and V. Petrov, *Opt. Lett.* **34**, 3053 (2009).
- S. C. Kumar, A. Agnesi, P. Dallochio, F. Pirzio, G. Reali, K. T. Zawilski, P. G. Schunemann, and M. Ebrahim-Zadeh, *Opt. Lett.* **36**, 3236 (2011).
- S. C. Kumar, A. Esteban-Martin, A. Santana, K. T. Zawilski, P. G. Schunemann, and M. Ebrahim-Zadeh, *Opt. Lett.* **41**, 3355 (2016).
- A. Hildenbrand, C. Kieleck, A. Tyazhev, G. Marchev, G. Stöppler, M. Eichhorn, P. G. Schunemann, V. L. Panyutin, and V. Petrov, *Opt. Eng.* **53**, 122511 (2014).
- S. Das, *Infrared Phys. Technol.* **69**, 13 (2015).
- S. Das, *Opt. Quantum Electron.* **51**, 70 (2019).
- K. L. Vodopyanov, F. Ganikhanov, J. P. Maffetone, I. Zwieback, and W. Ruderman, *Opt. Lett.* **25**, 841 (2000).
- G. Stoeppler, N. Thilmann, V. Pasiskevicius, A. Zukauskas, C. Canalias, and M. Eichhorn, *Opt. Express* **20**, 4509 (2012).
- G. Stoeppler, M. Schellhorn, and M. Eichhorn, *Laser Phys.* **22**, 1095 (2012).
- G. S. Edwards, *Laser Photonics Rev.* **3**, 545 (2009).
- R. Urschel, A. Borsutzky, and R. Wallenstein, *Appl. Phys. B: Lasers Opt.* **70**, 203 (2000).
- A. V. Smith, R. J. Gehr, and M. S. Bowers, *J. Opt. Soc. Am. B* **16**, 609 (1999).
- H. H. Pennes, *J. Appl. Physiol.* **85**, 5 (1998).
- A. L. McKenzie, *Phys. Med. Biol.* **35**, 1175 (1990).
- Y. Huang and J. U. Kang, *Proc. SPIE* **8209**, 82091W (2012).
- A. Vogel and V. Venugopalan, *Chem. Rev.* **103**, 577 (2003).